JCTC Journal of Chemical Theory and Computation

Article

Cite This: J. Chem. Theory Comput. 2019, 15, 3836−3843

pubs.acs.org/JCTC

# Structure and Dynamics of Water at the Water−Air Interface Using First-Principles Molecular Dynamics Simulations. II. NonLocal vs Empirical van der Waals Corrections

Mayank Dodia,[†] Tatsuhiko Ohto,[‡] Sho Imoto,[†] and Yuki Nagata*[,†]

[†]Max Planck Institute for Polymer Research, Ackermannweg 10, 55128 Mainz, Germany

[‡]Graduate School of Engineering Science, Osaka University, 1-3 Machikaneyama, Toyonaka, Osaka 560-8531, Japan

**ABSTRACT:** van der Waals (vdW) correction schemes have been recognized to be essential for an accurate description of liquid water in first-principles molecular dynamics simulation. The description of the structure and dynamics of water is governed by the type of the vdW corrections. So far, two vdW correction schemes have been often used: empirical vdW corrections and nonlocal vdW corrections. In this paper, we assess the influence of the empirical vs nonlocal vdW correction schemes on the structure and dynamics of water at the water−air interface. Since the structure of water at the water−air interface is established by a delicate balance of hydrogen bond formation and breaking, the simulation at the water−air interface provides a unique platform to testify as to the heterogeneous interaction of water. We used the metrics [Ohto et al. *J. Chem. Theory Comput.*, **2019**, *15*, 595−602] which are directly connected with the sum-frequency generation spectroscopic measurement. We find that the overall performance of nonlocal vdW methods is either similar or worse compared to the empirical vdW methods. We also investigated the performance of the optB88-DRSLL functional, which showed slightly less accuracy than the revPBE-D3 method. We conclude that the revPBE-D3 method shows the best performance for describing the interfacial water.

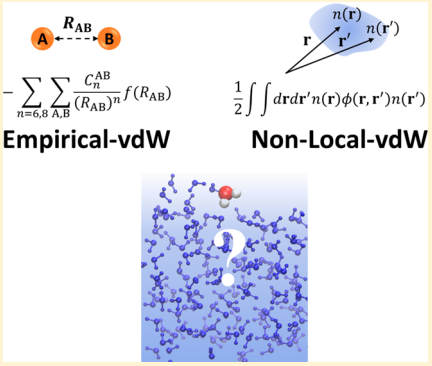


## 1. INTRODUCTION

van der Waals (vdW) interactions are essential for predicting structure and dynamics of water in the bulk and at the interface.[1,2] Although the density functional theory (DFT) itself is rigorous, the approximated exchange-correlation (XC) functionals within the generalized gradient approximation (GGA) or hybrid GGA cannot compute the vdW interaction energy accurately. Thus, first-principles molecular dynamics (FPMD) simulations performed with the GGA-XC or hybrid GGA-XC functionals erroneously predict the properties of water. For example, FPMD simulations based on the GGA-XC functionals without vdW corrections underestimated the bulk density of water. The underestimated density values of water in FPMD simulation is known to be improved largely by including the vdW corrections.[3−9] Analogously, the simulated values of the surface tensions of water at the water−air interface are drastically underestimated without the vdW corrections, whereas they are improved with the vdW corrections.[10,11] Since the impact of the vdW corrections is huge in predicting the properties of water, the choice of the vdW correction needs to be examined carefully.

So far, the frequently used vdW corrections in FPMD simulations of liquid water were the empirical vdW corrections based, in particular, on Grimme's D2[12] and D3[13−16] corrections. The D2 correction employs the environment-independent parameters for computing the vdW correction energy, while the D3 correction used the environment-dependent parameters. For both methods, the total DFT energy of a system, $E_{tot}$, within the GGA[17−19] can be expressed as

$$E_{tot} = T_s[n(\mathbf{r})] + E_{ext}[n(\mathbf{r})] + E_H[n(\mathbf{r})] + E_X^{GGA}[n(\mathbf{r})] + E_C^{GGA}[n(\mathbf{r})] + E^{empirical\text{-}vdW}(\mathbf{r}) \quad (1)$$

where $n(\boldsymbol{r})$ denotes the electron density, $T_s[n(\boldsymbol{r})]$ denotes the kinetic energy, $E_{ext}[n(\boldsymbol{r})]$ denotes the electron-nuclei interaction energy, $E_H[n(\boldsymbol{r})]$ denotes the electron−electron interaction energy, $E_X^{GGA}[n(\boldsymbol{r})]$ denotes the exchange energy of the GGA functional, $E_C^{GGA}[n(\boldsymbol{r})]$ denotes the correlation energy of the GGA functional, and $E^{empirical\text{-}vdW}(\mathbf{r})$ denotes the vdW correction energy based on the empirical vdW method. Since the empirical vdW corrections are computationally inexpensive (less than ∼20% of the computational cost of the base XC functional), they have been widely used for computing the properties of water.

Beyond the empirical vdW corrections, a computational scheme to evaluate the vdW correction energy within the DFT scheme has been proposed. This vdW correction scheme is called the nonlocal vdW (nl-vdW) correction scheme. The total DFT energy is given as:

$$E_{tot} = T_s[n(\mathbf{r})] + E_{ext}[n(\mathbf{r})] + E_H[n(\mathbf{r})] + E_X^{GGA}[n(\mathbf{r})] + E_C^{GGA/LDA}[n(\mathbf{r})] + E_C^{nl\text{-}vdW}[n(\mathbf{r})] \quad (2)$$

**Received:** March 11, 2019
**Published:** May 10, 2019




DOI: 10.1021/acs.jctc.9b00253
J. Chem. Theory Comput. 2019, 15, 3836−3843

where $E_C^{GGA/LDA}[n(r)]$ is the correlation energy calculated within the GGA or the local density approximation (LDA), and $E_C^{nl\text{-}vdW}[n(r)]$ denotes the correlation energy computed in the nl-vdW correction scheme. Since the nl-vdW corrections are calculated within the DFT framework through the electron density, the computational cost of GGA-FPMD simulations with nl-vdW corrections is more than doubled, compared with the GGA-FPMD simulation without any vdW corrections. The frequently used nl-vdW correction schemes are DRSLL[20,21] and rVV10.[22,23] The nl-vdW corrections were combined with various GGA XC functionals based on eq 2.[9,24−28] The DRSLL nl-vdW corrections have been used for predicting the property of bulk water.[25,26] Furthermore, the optB88-DRSLL[29] was suggested as one of the best DFT methods for computing the water properties.[1,9,24,30,31] However, the water properties in the bulk and at the interface predicted with the nl-vdW correction schemes have not been rigorously compared with those with the empirical vdW corrections.

Here, we evaluate various empirical vdW and nl-vdW corrections by focusing on the structure and dynamics of water at the water−air interface.[10,32−38] At the water−air interface, the free O−H (O−D) groups of the interfacial (heavy) water stick out, characterizing the structure of the interface.[32,33,39−44] Since the behavior of the free O−H (O−D) groups is well characterized by the surface-specific sum-frequency generation (SFG) spectroscopy technique,[45−51] we shall focus on the properties of the free O−H (O−D) groups. Furthermore, we also compute several bulk water properties. Based on the computed data, we make a ranking of the performance of the vdW correction schemes, with the similar scheme to ref 11. We find that the empirical D3 vdW correction scheme is comparably good as the rVV10 nl-vdW correction and better than the DRSLL nl-vdW correction. This indicates that the empirical vdW correction schemes are adequate to improve the description of interfacial water in FPMD simulation at the GGA level of theory.

## 2. VDW CORRECTIONS

**2.1. Environment-Independent Empirical vdW Corrections.** A simple description of the vdW correction employs environment-independent empirical vdW parameters. A typical vdW correction in this category is given by the Grimme's D2 model,[12] which can be written as

$$E^{\text{empirical-vdW,D2}} = -\sum_{A,B} \frac{s_6 C_6^{AB}}{(r_{AB})^6} f_{\text{damp}}(r_{AB}) \tag{3}$$

where $C_6^{AB}$ is the coefficient for atoms $A$ and $B$, $r_{AB}$ is the distance between $A$ and $B$, $s_6$ is a scaling factor, and $f_{\text{damp}}(r_{AB})$ is the short-range damping function. $C_6^{AB}$ is empirically determined and is independent of the local environment, making this correction scheme categorized into the environment-independent empirical vdW correction scheme.[52]

**2.2. Environment-Dependent Empirical vdW Corrections.** Straightforward extension of the Grimme's D2 correction is to make the coefficient $C^{AB}$ dependent on the local environment. The vdW correction schemes using the environment-dependent $C^{AB}(CN^A,CN^B)$ coefficients are called the environment-dependent empirical vdW correction,[52] where $CN^A$ and $CN^B$ stand for the coordination number for atoms $A$ and $B$, respectively. In this scheme, Grimme's D3 approach[13,14,16] has been used frequently. The vdW correction energy within the Grimme's D3 scheme is given by

$$E^{\text{empirical-vdW,D3}} = -\sum_{n=6,8}\sum_{A,B} \frac{s_n C_n^{AB}(CN^A, CN^B)}{(r_{AB})^n} f_{\text{damp}}^n(r_{AB}) + E^{(3)} \tag{4}$$

In addition to the environment-dependent $C^{AB}(CN^A,CN^B)$ coefficient, the D3 model differs from the D2 model in that the D3 model contains the higher order interactions term ($n = 8$) and the three-body interaction term ($E^{(3)}$).

The Grimme's D3 correction has mainly three versions: D3(0),[13] D3(BJ),[14] and D3m(BJ).[15] The D3(BJ) model uses a Becke-Johnson damping function[53] for short-range interactions, while the D3(0) model uses a Chai-Head-Gordon damping function.[54] The parameter set in the D3m(BJ) model was modified from the parameter set of the D3(BJ) model, by using a larger database of the conformational energy.[15]

**2.3. Nonlocal vdW Density Functional Correction Schemes.** The nl-vdW correction utilizes the DFT framework for computing long-range vdW interactions and without the need to define the pairwise interactions terms. The nonlocal correlational energy $E_C^{nl\text{-}vdW}[n(r)]$ can be written as

$$E_C^{\text{nl-vdW}}[n(\mathbf{r})] = \frac{1}{2}\int\int d\mathbf{r_1} d\mathbf{r_2} n(\mathbf{r_1})\phi(\mathbf{r_1}, \mathbf{r_2})n(\mathbf{r_2}) \tag{5}$$

where the correlation kernel $\phi$ is a function of the density $n(r)$ and the gradient of the density $\nabla n(r)$. The different versions of the nl-vdW correction arise from the different functional forms of $\phi$.[55−57]

So far, two popular nl-vdW correction schemes were presented: DRSLL[20,21] and rVV10.[22,23] For the DRSLL method presented by Dion and co-workers,[20] the nonlocal correlation kernel $\phi$ is directly derived using the plasmon-pole approximation and evaluated in terms of an auxiliary function $q = q(n(r),|\nabla n(r)|)$ in the DRSLL. On the other hand, the VV10 method was originally developed and revised by Vydrov and van Voorhis[22] and was optimized by Sabatini and co-workers,[23] which is called rVV10. The rVV10 utilizes a predefined empirical $\phi$ which has separate dependences for $n(r)$ and $\nabla n(r)$. In the rVV10 approach $\phi$ contains two parameters - $b$ and $C$: $b$ controls the short-range damping of asymptotic $\phi$, while $C$ controls the long-range behavior of $\phi$.[21,28,56]

In addition to the different functional forms of $\phi$, the DRSLL and rVV10 use different correlation energies; the DRSLL uses the correlation energy calculated within the LDA ($E_C^{LDA}$), while the rVV10 method uses the correlation energy calculated within the GGA ($E_C^{GGA}$).

## 3. SIMULATION PROTOCOLS

**3.1. FPMD Simulation.** We have performed Born−Oppenheimer simulations using the QUICKSTEP[58] method implemented in the CP2K code.[59] We have used Perdew−Burke−Ernzerhof (PBE)[60] and revised PBE (revPBE)[60,61] for the GGA XC functionals and Vosko-Wilk-Nusiar (VWN)[62] for the LDA correlation functional of the DRSLL method. This XC functional energy is combined with empirical vdW correction schemes using Grimme's D2,[12] D3(0),[13] D3(BJ),[14] and D3m(BJ),[15] as well as the nl-vdW correction schemes using the DRSLL[20,21] and rVV10.[22,23] Furthermore, we tested the optB88-DRSLL method.[19,29] The resulting calculation methods and their notations are listed in Table 1.

We have used a triple $\zeta$ valence Gaussian basis set with two sets of polarization functions (TZV2P). Norm-conserving Goedecker-Teter-Hutter pseudopotentials[63,64] were used to describe the core electrons. We utilized the self-consistent field


DOI: 10.1021/acs.jctc.9b00253
J. Chem. Theory Comput. 2019, 15, 3836−3843

**Table 1. List of Simulations Methods Discussed**

| notation | exchange | correlation | vdW correction | remarks |
|---|---|---|---|---|
| PBE[a] | PBE | PBE | | |
| PBE-D2[a] | PBE | PBE | D2[b] | |
| PBE-D3(0)[a] | PBE | PBE | D3(0)[c] | |
| PBE-D3(BJ)[a] | PBE | PBE | D3(BJ)[d] | |
| PBE-D3m(BJ) | PBE | PBE | D3m(BJ)[e] | |
| PBE-DRSLL | PBE | VWN | DRSLL[f] | |
| PBE-rVV10 | PBE | PBE | rVV10[g] | $b$ = 6.6, $C$ = 0.0093 |
| revPBE[a] | revPBE | PBE | | |
| revPBE-D2 | revPBE | PBE | D2[b] | |
| revPBE-D3(0)[a] | revPBE | PBE | D3(0)[c] | |
| revPBE-D3(BJ)[a] | revPBE | PBE | D3(BJ)[d] | |
| revPBE-DRSLL | revPBE | VWN | DRSLL[f] | |
| revPBE-rVV10 | revPBE | PBE | rVV10[g] | $b$ = 3.7, $C$ = 0.0093 |
| optB88-DRSLL | optB88[h] | VWN | DRSLL[f] | |

[a]The data are obtained from our previous work.[11] [b]Reference 12. [c]Reference 13. [d]Reference 14. [e]Reference 15. [f]Reference 20. [g]Reference 22. [h]Reference 29.

(SCF) cutoff of $2 \times 10^{-7}$ hartrees and kinetic energy density cutoff set at $1 \times 10^{-10}$. The plane wave density cutoff was set to 320 Ry. To accelerate the MD simulations, $D_2O$ was used instead of $H_2O$, and the time step was set to 0.5 fs. All simulations were performed at 300 K in the NVT ensemble with the CSVR themostat.[65] We used 160 $D_2O$ molecules in a simulation cell $(L_x, L_y, L_z)$ = (16.63 Å, 16.63 Å, 44.10 Å), where the water−air interface is parallel to the $xy$ plane and the surface normal is parallel to the $z$-axis. The cutoff of the vdW interactions was set to 10 Å. We ran 10 independent simulations from previously generated configurations from the revPBE-D3(0) functional for revPBE+vdW simulations and the PBE-D3(0) functional for PBE+vdW and optB88-DRSLL simulations. Fifteen ps of the production run was generated after 5 ps equilibration runs. Configurations were captured at every 10th step (i.e., at 5 fs) and were used for analysis.

**3.2. POLI2VS MD Simulation.** We generated the reference bulk and interfacial data from the MD trajectory with the POLI2VS model.[66] The details for the simulations have been provided previously.[11] The POLI2VS polarizable water model is the most tested water model at the water−air interface, through the direct comparison between the SFG measurement and SFG simulation.[33,66−73] Furthermore, the direct comparison of the POLI2VS model and another accurate model (MB-pol) shows that the description of interfacial water given by POLI2VS and MB-pol models is within the error bars.[33] Thus, we used the POLI2VS model to generate the reference data.

## 4. TARGET QUANTITIES

**4.1. Density Profile of Interfacial Water.** The bulk water density $\rho_0$ (at zero pressure) can be calculated by fitting the density profile in the water slab system to the hyperbolic tangent function $\rho(z)$ along the surface normal ($z$-axis)

$$\rho(z) = \frac{\rho_0}{2}\left(1 - \tanh\left(-\frac{|z| - |z_G|}{\delta}\right)\right) \quad (6)$$

where $z_G$ is the $z$-coordinate of the Gibbs dividing surface, and $\delta$ is the interfacial thickness parameter. For this calculation, the center of mass of the water slab was set at the origin of the $z$-axis, and the deuterium atoms in $D_2O$ were replaced by hydrogen atoms. Note that $\rho_0$ calculated in the slab model agrees well with the density calculated in the NPT ensemble within the error. In fact, the water density predicted in the slab model ($0.989 \pm 0.001$ g/cm$^3$)[11] is very close to the density predicted in the NPT ensemble ($0.993 \pm 0.001$ g/cm$^3$)[66] in the MD simulation with the POLI2VS force field model.

**4.2. Fraction of Interfacial Water Molecules with the Free O−D Group and the Angle of the Free O−D Group.** An O−D group of the $D_2O$ molecule in the interfacial region is defined as free, when the intermolecular O···O distance of its oxygen atom and oxygen atom of any other water molecule is greater than 3.5 Å and the D−O···O angle is more than 50°.[32] Otherwise, an O−D group is defined as being hydrogen-bonded. The interfacial region for the slab system is defined along the $z$-axis as[45]

$$z_G - 3.11\ \text{Å} \le |z| \le z_G + 3.11\ \text{Å} \quad (7)$$

The fraction of the interfacial free O−D groups is calculated as the sum of the DA and DAA fractions, which have been defined elsewhere.[11,32] The fraction of the free O−D group estimated from the previously generated reference POLI2VS value is 28%, which is in good agreement with SFG spectroscopy measurements of 20−25%.[45,74] We can also calculate the averaged angle $\langle\theta\rangle$, formed by the free O−D groups and the surface normal. This value can also be extracted using polarization-dependent SFG spectroscopy.[33,47−49,75−77]

**4.3. Lifetime of the Free O−D Group.** The lifetime of the free O−D group is computed using the time correlation function

$$C(t) = \frac{\langle \prod_0^t h(t')\rangle}{\langle h(0)\rangle} \quad (8)$$

where $h(t)$ is defined as 1 when an O−D group is free at time $t$, otherwise 0. $C(t)$ is fitted using the double exponential form[78]

$$C(t) = ae^{-(t/\tau_f)} + be^{-(t/\tau_s)} + c \quad (9)$$

within the time region 0−5 ps, where $a$, $b$, and $c$ are the fitting coefficients. The time constants $\tau_f$ and $\tau_s$ denote the fast and slow decays, respectively. $\tau_f$ is governed by the librational motion of water, while $\tau_s$ is governed by the motion that the free O−D group rotates and forms a hydrogen bond at the water−air interface. These values can be probed using time-resolved SFG spectroscopy,[41,72,79] whereas so far only the lifetime of the free O−H group has been obtained[41] and the lifetime of the free O−D group is not determined. As the POLI2VS simulation agrees with the experimental data for $H_2O$,[32] we used the POLI2VS data of $D_2O$ as the reference.

**4.4. Radial Distribution Function (RDF).** The oxygen−oxygen RDF $g_{OO}(r)$ was calculated when the reference oxygen atom of a water molecule is in the region $|z| \le 1.35$ Å of the slab model. The RDF was calculated based on the computed $\rho_0$. The resolution of the RDF, $\Delta r$, was set as 0.1 Å.

## 5. RESULTS

The obtained data is summarized in Table 2 with the earlier evaluated values for the PBE and revPBE with and without vdW corrections.

**5.1. Bulk Water Density.** First, we compare the obtained density values with the reported value. As is mentioned in ref 11,


DOI: 10.1021/acs.jctc.9b00253
J. Chem. Theory Comput. 2019, 15, 3836−3843

Table 2. Bulk and Interfacial Water Data Using Various DFT+vdW Methods[a]

| | optB88-DRSLL | PBE | | | | | | revPBE | | | | | | POLI2VS | exp. |
|---|---|---|---|---|---|---|---|---|---|---|---|---|---|---|---|
| | | none | D2 | D3(0) | D3(BJ) | D3m(BJ) | DRSLL | rVV10 | none | D2 | D3(0) | D3(BJ) | DRSLL | rVV10 | | |
| $\rho$ (g/cm$^3$) | 1.07 | 0.91 | 1.02 | 1.03 | 1.00 | 1.00 | 1.12 | 1.03 | 0.69 | 0.94 | 0.94 | 0.93 | 0.93 | 1.06 | 0.99 | 1.00 |
| $z_G$ (Å) | 8.08 | 9.50 | 8.43 | 8.44 | 8.70 | 8.63 | 7.70 | 8.36 | 12.5 | 9.22 | 9.18 | 9.31 | 9.31 | 8.14 | 8.76 | |
| $\delta$ (Å) | 1.02 | 1.08 | 1.06 | 1.01 | 1.05 | 1.02 | 0.81 | 0.96 | 2.06 | 1.06 | 1.17 | 1.16 | 1.06 | 1.03 | 1.29 | |
| DA (%) | 7 | 12 | 7 | 8 | 9 | 9 | 6 | 7 | 27 | 12 | 11 | 14 | 19 | 9 | 12 | |
| DAA (%) | 13 | 15 | 12 | 13 | 14 | 13 | 14 | 13 | 11 | 14 | 13 | 14 | 17 | 13 | 16 | |
| DDA (%) | 16 | 17 | 17 | 17 | 17 | 17 | 17 | 17 | 13 | 18 | 17 | 18 | 19 | 17 | 17 | |
| free OH (%) | 20 | 27 | 19 | 21 | 22 | 22 | 20 | 19 | 38 | 26 | 24 | 28 | 35 | 23 | 28 | |
| <$\vartheta$> (deg) | 52 | 54 | 51 | 53 | 51 | 55 | 56 | 48 | 76 | 65 | 66 | 65 | 72 | 56 | 61 | |
| $\tau_f$ (ps) | 0.15 | 0.19 | 0.16 | 0.15 | 0.18 | 0.17 | 0.09 | 0.21 | 0.19 | 0.12 | 0.11 | 0.15 | 0.10 | 0.14 | 0.11 | |
| $\tau_s$ (ps) | 1.69 | 2.18 | 1.99 | 1.87 | 2.04 | 1.86 | 1.00 | 2.42 | 1.05 | 1.03 | 1.06 | 1.25 | 0.51 | 1.48 | 1.02 | 1.1[b] |
| $h_{max}$ | 3.12 | 3.67 | 3.62 | 3.44 | 3.78 | 3.69 | 2.54 | 3.73 | 2.74 | 2.97 | 2.72 | 3.12 | 2.18 | 2.95 | 2.73 | 2.58[c] |
| $r_{max}$ (Å) | 2.75 | 2.75 | 2.71 | 2.72 | 2.71 | 2.71 | 2.82 | 2.70 | 2.86 | 2.77 | 2.81 | 2.77 | 2.92 | 2.74 | 2.78 | 2.80[c] |
| $h_{min}$ | 0.62 | 0.18 | 0.31 | 0.36 | 0.18 | 0.21 | – | 0.23 | 0.46 | 0.56 | 0.69 | 0.42 | – | 0.67 | 0.83 | 0.84[c] |
| $r_{min}$ (Å) | 3.24 | 3.36 | 3.25 | 3.26 | 3.27 | 3.28 | – | 3.24 | 3.61 | 3.42 | 3.46 | 3.36 | – | 3.23 | 3.43 | 3.47[c] |

[a]The average error bars for $\rho$, $z_G$, $\delta$, fractions, $\langle\vartheta\rangle$, $\tau_f$, $\tau_s$, $h_{max}$, $r_{max}$, $h_{min}$, and $r_{min}$ are 0.01 g/cm$^3$, 0.1 Å, 0.2 Å, 1.0%, 1.5 degrees, 0.01 ps, 0.2 ps, 0.1, 0.01 Å, 0.4, and 0.02 Å, respectively. [b]Reference 32. [c]Reference 83.

the density of water simulated with the D3 vdW correction agrees with the previous reports. On the other hand, the calculated density value with the nl-vdW correction has not been so much reported. The bulk water density for the PBE-DRSLL ($\rho$ = 1.12 ± 0.01 g/cm$^3$) is similar to the reported values of 1.13 g/cm$^3$ in ref 26 and 1.18 g/cm$^3$ in ref 28. However, our data for the revPBE-DRSLL differs from the data in ref 26; we obtained $\rho$ = 0.93 ± 0.01 g/cm$^3$, smaller than the value of 1.02 g/cm$^3$.[26] This can be rationalized by the different techniques to compute the density of water. We used the slab model in the NVT ensemble, while ref 26 used the computed the pressure−density relation and estimated the density at 1 atm. As is mentioned above, we have already checked that the water density predicted in the slab model is very close to the density predicted in the NPT ensemble. Together with the very good agreement with our estimation of the water density in the slab model with that in the NPT simulation in the GGA+D3 level of theory,[11] we believe that the water density at the revPBE-DRSLL level of theory is 0.93 ± 0.01 g/cm$^3$. We would like to note that, to the best of our knowledge, simulated density of water using the PBE-rVV10 and revPBE-rVV10 methods has not been reported yet.

Now, we turn our focus on the effects of various vdW corrections on the bulk water density. Table 2 indicates that, compared with the FPMD simulation without the vdW corrections, the density values are improved with the vdW corrections, while there is no clear trend that the nl-vdW correction scheme provides better density value than empirical vdW corrections. In fact, the PBE-DRSLL level of theory provides the largest deviation from the reference value of 0.989 g/cm$^3$.

**5.2. Interfacial Thickness.** For the interfacial thickness $\delta$, the tendency is consistent with the bulk water density. The thickness parameter decreases with any type of the vdW correction schemes, making the thickness parameter closer to the reference value of 1.292 Å. On the other hand, we could not see a signature that the nl-vdW corrections provide the better thickness value than the empirical vdW corrections. Again, the largest deviation from the reference value is obtained at the PBE-DRSLL level of theory.

**5.3. Fraction of Interfacial Water Molecules with Free O−D Groups.** Here, we discuss the effect of the vdW corrections on the fraction of the interfacial water molecules with the free O−D groups (DA-type and DAA-type water conformation). For the PBE and revPBE cases, the fraction of DA water molecules decreases drastically with any type of the vdW correction schemes, while the fraction of DAA is rather insensitive to the vdW corrections. Interestingly, the PBE-DRSLL drastically underestimated the DA fraction (6%), while the revPBE-DRSLL overestimated the DA fraction significantly (19%). As a result, the DRSLL correction provides noticeably scattered values of the DA fraction. The rVV10 method predicts the DA fraction closer to the reference value than the DRSLL, whereas it is worse than the empirical D3 vdW corrections. Overall, we conclude that the prediction of the free O−D fraction with the nl-vdW corrections is less accurate than that with the empirical D3 vdW corrections.

**5.4. Angle of the Free O−D Group of Interfacial Water Molecules.** We do not see any systematic trend on the effects of the vdW correction on the free O−D angle $\langle\theta\rangle$ of the interfacial water molecules. However, it is worth mentioning that the worst prediction of the free O−D angle with the PBE XC functional is given by the rVV10 nl-vdW correction scheme, while the worst prediction with the revPBE XC functional is given by the



DOI: 10.1021/acs.jctc.9b00253
J. Chem. Theory Comput. 2019, 15, 3836−3843

DRSLL nl-vdW correction scheme. As a result, we conclude that the use of the nl-vdW correction scheme does not improve the description of the free O−D angle over the empirical vdW corrections.

**5.5. Lifetime of Free O−D Groups.** We computed the time correlation function for the free O−D group at the water−air interface and obtained the lifetime of the free O−D group from the fit of eq 9. Figure 1 displays the time correlation function

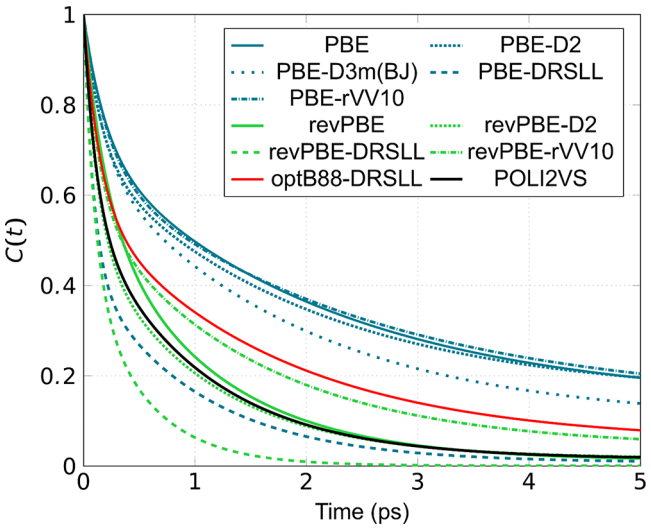


**Figure 1.** Time correlation functions of the free O−D group of the interfacial water molecules.

$C(t)$ for the DFT XC functionals, and Table 2 summarizes the fitted time constants. The fast time scale ($\tau_f$) is in the range of 0.1−0.2 ps, while the slow time scale ($\tau_s$), which is associated with the motion of the free O−D rotation and formation of a new hydrogen bond, is scattered from 0.5 to 2.4 ps. We discuss the behavior of the slow time scale in more detail.

In our previous report,[11] the dynamics of the free O−D group is strongly affected by the XC functional rather than the vdW corrections. This trend can be seen in the current data except for the DRSLL vdW correction; $\tau_s$ calculated with the DRSLL correction is almost half of $\tau_s$ with the D3(0) vdW correction. This is likely due to an underestimation of the hydrogen bond strength in the DRSLL method.[80,81] Indeed, this is in line with the results of hydrogen bond dynamics in ref 9, where Klein and co-workers have reported that the lifetime of the hydrogen bond is 5.0 ps at the PBE-D3(0) level of theory and 1.0 ps at the PBE-DRSLL level of theory. As such, we conclude that the interfacial water dynamics is mainly governed by the XC functional and thus the effect of the vdW correction is minor, except for the DRSLL correction.

**5.6. RDF.** We plot $g_{OO}(r)$ in Figure 2 and summarize the heights and positions of the first maxima ($h_{max}$;$r_{max}$) and minima ($h_{min}$;$r_{min}$) in Table 2. First, we compare our simulated data with the previous reports. The RDF with the empirical D2 and D3 correction schemes has been reported in many papers,[3,9,34,82] and our data is consistent with this literature. In contrast, the RDF data with the nl-vdW corrections are available only for the DRSLL correction. For the simulation at the PBE-DRSLL level of theory, it was reported that $h_{max}$ = 2.77 and $r_{max}$ = 2.80 Å at 295 K in ref 24 and $h_{max}$ = 2.51 and $r_{max}$ = 2.80 Å at 295 K in ref 28. These agree with $h_{max}$ = 2.54 and $r_{max}$ = 2.82 Å in our simulation. $h_{max}$ = 2.18 and $r_{max}$ = 2.92 Å in our simulation at the revPBE-

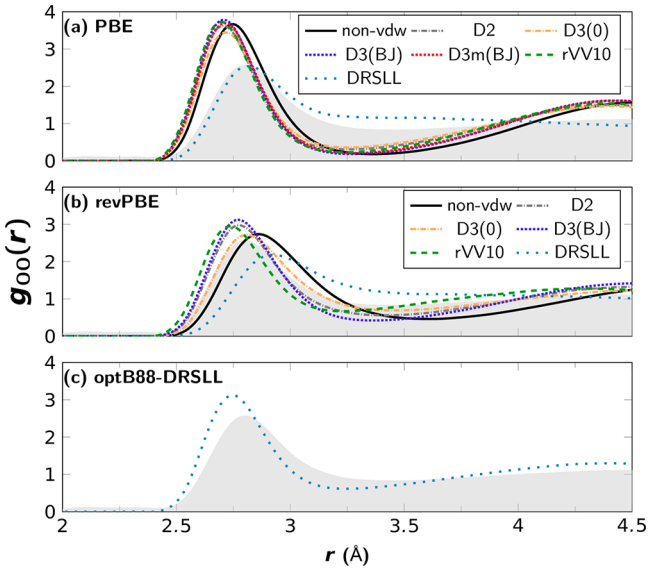


**Figure 2.** Oxygen−oxygen RDF of water simulated in the FPMD simulation with the (a) PBE XC functional, (b) revPBE XC functional, and (c) optB88-DRSLL level of theory. The shaded area represents the experimental data from X-ray diffraction measurements.[83]

DRSLL level of theory are corroborated by previously reported values of $h_{max}$ = 2.35 and $r_{max}$ = 2.92 Å at 300 K in ref 24. Furthermore, one can see that $g_{OO}(r)$ simulated with the DRSLL correction scheme does not show a clear RDF minimum, indicating that the water structure is disordered excessively. This is consistent with ref 26.

The data in Table 2 indicates that the RDF data is sensitive to the XC functional and is rather insensitive to the vdW corrections, except for the DRSLL correction. The DRSLL corrections drastically reduce $h_{max}$.

**5.7. Performance of the optB88-DRSLL Functional.** The optB88-DRSLL functional was developed by Michaelides and co-workers[29] based on the original B88 exchange functional.[19] This functional is known to predict the energy of water and ice clusters well.[1] Furthermore, RDF[9,24] and dipole moment[24] obtained from the optB88-DRSLL simulation of bulk water is in good agreement with the experimental data. The reported bulk water density in the simulation at the optB88-DRSLL level of theory was 1.08 g/cm$^3$ at 295 K and 1 atm,[25] which is consistent with our density value of $\rho$ = 1.07 ± 0.02 g/cm$^3$. This density value is higher than the experimental value of $\rho$ = 1.00 g/cm$^3$. As such, the performance of the optB88-DRSLL in the bulk is good but still far from being perfect.

How about the description of the optB88-DRSLL level of theory for the water−air interface? The fraction of the interfacial water molecules with the free O−D groups is 20%, which is much lower than the reference value of 28%. The angle formed by the free O−D group and surface normal is $\langle\theta\rangle$ = 52°, which is also drastically underestimated. Figure 2 indicates that the optB88-DRSLL predicts slower free O−D group dynamics ($\tau_s$ = 1.69 ps). As such, we conclude that, within the metric defined in this study for air−water interface, the performance of the optB88-DRSLL level of theory is not so good.

**5.8. Performance Ranking.** Based on the above data, we can rank the performance of various DFT+vdW methods, in terms of the metrics of the simulated air−water interface. This is done by using the following equation


DOI: 10.1021/acs.jctc.9b00253
J. Chem. Theory Comput. 2019, 15, 3836−3843

**Table 3. Score of Various DFT+vdW Functionals for Bulk and Interfacial Data**

| | | PBE | | | | | | | revPBE | | | | | |
|---|---|---|---|---|---|---|---|---|---|---|---|---|---|---|
| | optB88-DRSLL | none | D2 | D3(0) | D3(BJ) | D3m(BJ) | DRSLL | rVV10 | none | D2 | D3(0) | D3(BJ) | DRSLL | rVV10 |
| $\rho$ | 0.66 | 0.90 | 0.22 | 0.28 | 0.05 | 0.02 | 1.16 | 0.32 | 2.98 | 0.59 | 0.57 | 0.70 | 0.70 | 0.60 |
| $\delta$ | 0.96 | 0.73 | 0.81 | 0.96 | 0.83 | 0.96 | 1.67 | 1.16 | 2.69 | 0.80 | 0.40 | 0.47 | 0.82 | 0.91 |
| fraction | 1.33 | 0.15 | 1.46 | 1.22 | 0.94 | 1.04 | 1.40 | 1.44 | 1.75 | 0.29 | 0.62 | 0.04 | 1.26 | 0.90 |
| $<\vartheta>$ | 1.05 | 0.85 | 1.27 | 0.95 | 1.26 | 0.81 | 0.58 | 1.52 | 1.71 | 0.39 | 0.47 | 0.37 | 1.25 | 0.62 |
| $\tau_s$ | 1.20 | 2.09 | 1.74 | 1.52 | 1.83 | 1.51 | 0.04 | 2.51 | 0.06 | 0.02 | 0.07 | 0.42 | 0.91 | 0.83 |
| $h_{max}$ | 1.08 | 2.15 | 2.07 | 1.71 | 2.38 | 2.21 | 0.07 | 2.27 | 0.32 | 0.79 | 0.28 | 1.08 | 0.78 | 0.75 |
| $r_{max}$ | 0.77 | 0.77 | 1.39 | 1.24 | 1.39 | 1.39 | 0.31 | 1.54 | 0.93 | 0.46 | 0.15 | 0.46 | 1.85 | 0.93 |
| $h_{min}$ | 1.16 | 3.43 | 2.75 | 2.49 | 3.41 | 3.28 | – | 3.17 | 1.97 | 1.45 | 0.75 | 2.17 | – | 0.88 |
| $r_{min}$ | 1.98 | 0.95 | 1.89 | 1.81 | 1.72 | 1.63 | – | 1.98 | 1.20 | 0.43 | 0.09 | 0.95 | – | 2.06 |
| final score | 1.07 | 1.09 | 1.25 | 1.12 | 1.19 | 1.08 | 0.82 | 1.53 | 1.72 | 0.48 | 0.41 | 0.53 | 0.93 | 0.84 |

$$\kappa_i^j = \frac{|\chi_i^j - \chi_i^{ref}|}{\sigma_i} \quad (10)$$

where $\kappa_i^j$ is the score of the method $j = \{$optB88, revPBE, revPBE-D3(0), revPBE-D3(BJ), revPBE-DRSLL, revPBE-rVV10, PBE, PBE-D3(0), PBE-D3(BJ), PBE-D3m(BJ), PBE-DRSLL, PBE-rVV10$\}$ for the calculated property $i = \{\rho$, interfacial free O−D fraction, $\langle\theta\rangle$, $\tau_s$, $g_{OO}(r)\}$. $\chi_i^j$ denotes the value of the quantity $i$ computed with the method $j$, $\chi_i^{ref}$ is the reference value of the quantity $i$, and $\sigma_i$ is the standard deviation of quantity $i$ for all methods in set $j$. The ranking for $g_{OO}(r)$ for the method $j$ was calculated using the average ranking for individual components of $g_{OO}(r)$, i.e., the set $\{h_{max}, r_{max}, h_{min}, r_{min}\}$. Using the above expression, a smaller value $\kappa_i^j$ implies better performance by method $j$ for quantity $i$. For all values except density ($\chi_\rho^{ref} = 1.00$ g/cm$^3$) and $g_{OO}(r)$, the data obtained from the POLI2VS MD simulation results have been taken as the reference values.

Table 3 shows the performance ranking for the DFT+vdW methods used in this study. While the average nl-vdW functional score (1.03) is close to the empirical vdW (0.87), the score of the best performing nl-vdW method, i.e., revPBE-rVV10 (0.84), is much larger than the revPBE-D3(0) functional score (0.41). This illustrates that the overall performance of DFT-nl-vdW methods is either similar or worse than empirical vdW methods. nl-vdW methods enhance the bulk water density when compared to non-vdW corrected functionals, but the interfacial description of water is either similar or worse when compared to empirical vdW methods.

## 6. CONCLUSION

We tested the efficacy of two different classes of vdW models: environment-dependent empirical corrections and nonlocal vdW functionals for a description of the air−water interface. By using a scoring scheme which ranks the DFT+vdW functionals based on bulk water density, interfacial width, interfacial free O−D group fraction, interfacial free O−D lifetime decay, and oxygen−oxygen radial distribution function, we were able to study the effect of nl-vdW methods on the air−water interface. We concluded that within the margin of error both nl-vdW methods (optB88-DRSLL and rVV10) show a similar or worse description for interfacial water as compared to the empirical D2 and D3 vdW methods. Our data clearly indicates that the revPBE+D3 models are much better suited for simulating the air−water interface, while the nl-vdW methods perform similarly to the PBE functional.

Finally, we would like to note that our results do not indicate that the nl-vdW corrections have no opportunity to describe the water dynamics accurately. Rather, our data illustrate that the current nl-vdW correction schemes are not well optimized, and thus further fine-tuning of the nl-vdW schemes for an accurate description of the air−water interface will be required.

## AUTHOR INFORMATION


### Corresponding Author

*E-mail: nagata@mpip-mainz.mpg.de.

### ORCID

Mayank Dodia: 0000-0001-8533-885X

Tatsuhiko Ohto: 0000-0001-8681-3800

Yuki Nagata: 0000-0001-9727-6641



### Funding

We acknowledge the financial support from the MaxWater project of the Max Planck Society. The computations were performed at a local computing cluster at the Max Planck Institute for Polymer Research and at the Max Planck Computing and Data Facility.


### Notes

The authors declare no competing financial interest.

## REFERENCES


(1) Gillan, M. J.; Alfè, D.; Michaelides, A. Perspective: How Good Is DFT for Water? *J. Chem. Phys.* **2016**, *144*, 130901.

(2) Morawietz, T.; Singraber, A.; Dellago, C.; Behler, J. *Proc. Natl. Acad. Sci. U. S. A.* **2016**, *113*, 8368−8373.

(3) Lin, I. C.; Seitsonen, A. P.; Tavernelli, I.; Rothlisberger, U. Structure and Dynamics of Liquid Water from Ab Initio Molecular Dynamics-Comparison of BLYP, PBE, and RevPBE Density Functionals with and without van Der Waals Corrections. *J. Chem. Theory Comput.* **2012**, *8*, 3902−3910.

(4) Lin, I.-C.; Seitsonen, A. P.; Coutinho-Neto, M. D.; Tavernelli, I.; Rothlisberger, U. Importance of van Der Waals Interactions in Liquid Water. *J. Phys. Chem. B* **2009**, *113*, 1127−1131.

(5) Ma, Z.; Zhang, Y.; Tuckerman, M. E. Ab Initio Molecular Dynamics Study of Water at Constant Pressure Using Converged Basis Sets and Empirical Dispersion Corrections. *J. Chem. Phys.* **2012**, *137*, 044506.

(6) Marsalek, O.; Markland, T. E. Ab Initio Molecular Dynamics with Nuclear Quantum Effects at Classical Cost: Ring Polymer Contraction for Density Functional Theory. *J. Chem. Phys.* **2016**, *144*, 054112.

(7) Chen, M.; Ko, H.-Y.; Remsing, R. C.; Calegari Andrade, M. F.; Santra, B.; Sun, Z.; Selloni, A.; Car, R.; Klein, M. L.; Perdew, J. P.; et al. Ab Initio Theory and Modeling of Water. *Proc. Natl. Acad. Sci. U. S. A.* **2017**, *114*, 10846−10851.

(8) Ruiz Pestana, L.; Mardirossian, N.; Head-Gordon, M.; Head-Gordon, T. Ab Initio Molecular Dynamics Simulations of Liquid Water Using High Quality Meta-GGA Functionals. *Chem. Sci.* **2017**, *8*, 3554−3565.




DOI: 10.1021/acs.jctc.9b00253
*J. Chem. Theory Comput.* 2019, 15, 3836−3843

(9) Bankura, A.; Karmakar, A.; Carnevale, V.; Chandra, A.; Klein, M. L. Structure, Dynamics, and Spectral Diffusion of Water from First-Principles Molecular Dynamics. *J. Phys. Chem. C* **2014**, *118*, 29401−29411.
(10) Nagata, Y.; Ohto, T.; Bonn, M.; Kühne, T. D. Surface Tension of Ab Initio Liquid Water at the Water-Air Interface. *J. Chem. Phys.* **2016**, *144*, 204705.
(11) Ohto, T.; Dodia, M.; Imoto, S.; Nagata, Y. Structure and Dynamics of Water at the Water−Air Interface Using First-Principles Molecular Dynamics Simulations within Generalized Gradient Approximation. *J. Chem. Theory Comput.* **2019**, *15*, 595−602.
(12) Grimme, S. Semiempirical GGA-Type Density Functional Constructed with a Long-Range Dispersion Correction. *J. Comput. Chem.* **2006**, *27*, 1787−1799.
(13) Grimme, S.; Antony, J.; Ehrlich, S.; Krieg, H. A Consistent and Accurate Ab Initio Parametrization of Density Functional Dispersion Correction (DFT-D) for the 94 Elements H-Pu. *J. Chem. Phys.* **2010**, *132*, 154104.
(14) Grimme, S.; Ehrlich, S.; Goerigk, L. Effect of the Damping Function in Dispersion Corrected Density Functional Theory. *J. Comput. Chem.* **2011**, *32*, 1456−1465.
(15) Smith, D. G. A.; Burns, L. A.; Patkowski, K.; Sherrill, C. D. Revised Damping Parameters for the D3 Dispersion Correction to Density Functional Theory. *J. Phys. Chem. Lett.* **2016**, *7*, 2197−2203.
(16) Grimme, S.; Hansen, A.; Brandenburg, J. G.; Bannwarth, C. Dispersion-Corrected Mean-Field Electronic Structure Methods. *Chem. Rev.* **2016**, *116*, 5105−5154.
(17) Langreth, D. C.; Mehl, M. J. Beyond the Local-Density Approximation in Calculations of Ground-State Electronic Properties. *Phys. Rev. B: Condens. Matter Mater. Phys.* **1983**, *28*, 1809−1834.
(18) Perdew, J. P.; Chevary, J. A.; Vosko, S. H.; Jackson, K. A.; Pederson, M. R.; Singh, D. J.; Fiolhais, C. Atoms, Molecules, Solids, and Surfaces: Applications of the Generalized Gradient Approximation for Exchange and Correlation. *Phys. Rev. B: Condens. Matter Mater. Phys.* **1992**, *46*, 6671−6687.
(19) Becke, A. D. Density-Functional Exchange-Energy Approximation with Correct Asymptotic Behavior. *Phys. Rev. A: At., Mol., Opt. Phys.* **1988**, *38*, 3098−3100.
(20) Dion, M.; Rydberg, H.; Schröder, E.; Langreth, D. C.; Lundqvist, B. I. Van Der Waals Density Functional for General Geometries. *Phys. Rev. Lett.* **2004**, *92*, 246401.
(21) Román-Pérez, G.; Soler, J. M. Efficient Implementation of a van Der Waals Density Functional: Application to Double-Wall Carbon Nanotubes. *Phys. Rev. Lett.* **2009**, *103*, 096102.
(22) Vydrov, O. A.; Van Voorhis, T. Nonlocal van Der Waals Density Functional: The Simpler the Better. *J. Chem. Phys.* **2010**, *133*, 244103.
(23) Sabatini, R.; Gorni, T.; de Gironcoli, S. Nonlocal van Der Waals Density Functional Made Simple and Efficient. *Phys. Rev. B: Condens. Matter Mater. Phys.* **2013**, *87*, 041108.
(24) Zhang, C.; Wu, J.; Galli, G.; Gygi, F. Structural and Vibrational Properties of Liquid Water from van Der Waals Density Functionals. *J. Chem. Theory Comput.* **2011**, *7*, 3054−3061.
(25) Del Ben, M.; Hutter, J.; VandeVondele, J. Probing the Structural and Dynamical Properties of Liquid Water with Models Including Non-Local Electron Correlation. *J. Chem. Phys.* **2015**, *143*, 054506.
(26) Wang, J.; Román-Pérez, G.; Soler, J. M.; Artacho, E.; Fernández-Serra, M.-V. Density, Structure, and Dynamics of Water: The Effect of van Der Waals Interactions. *J. Chem. Phys.* **2011**, *134*, 024516.
(27) Peng, H.; Yang, Z.-H.; Perdew, J. P.; Sun, J. Versatile van Der Waals Density Functional Based on a Meta-Generalized Gradient Approximation. *Phys. Rev. X* **2016**, *6*, 041005.
(28) Corsetti, F.; Artacho, E.; Soler, J. M.; Alexandre, S. S.; Fernández-Serra, M.-V. Room Temperature Compressibility and Diffusivity of Liquid Water from First Principles. *J. Chem. Phys.* **2013**, *139*, 194502.
(29) Klimeš, J.; Bowler, D. R.; Michaelides, A. Chemical Accuracy for the van Der Waals Density Functional. *J. Phys.: Condens. Matter* **2010**, *22*, 022201.
(30) Carrasco, J.; Santra, B.; Klimeš, J.; Michaelides, A. To Wet or Not to Wet? Dispersion Forces Tip the Balance for Water Ice on Metals. *Phys. Rev. Lett.* **2011**, *106*, 026101.
(31) Tocci, G.; Joly, L.; Michaelides, A. Friction of Water on Graphene and Hexagonal Boron Nitride from Ab Initio Methods: Very Different Slippage despite Very Similar Interface Structures. *Nano Lett.* **2014**, *14*, 6872−6877.
(32) Tang, F.; Ohto, T.; Hasegawa, T.; Xie, W. J.; Xu, L.; Bonn, M.; Nagata, Y. Definition of Free O-H Groups of Water at the Air-Water Interface. *J. Chem. Theory Comput.* **2018**, *14*, 357−364.
(33) Sun, S.; Tang, F.; Imoto, S.; Moberg, D. R.; Ohto, T.; Paesani, F.; Bonn, M.; Backus, E. H. G.; Nagata, Y. Orientational Distribution of Free O-H Groups of Interfacial Water Is Exponential. *Phys. Rev. Lett.* **2018**, *121*, 246101.
(34) Galib, M.; Duignan, T. T.; Misteli, Y.; Baer, M. D.; Schenter, G. K.; Hutter, J.; Mundy, C. J. Mass Density Fluctuations in Quantum and Classical Descriptions of Liquid Water. *J. Chem. Phys.* **2017**, *146*, 244501.
(35) Nagata, Y.; Ohto, T.; Backus, E. H. G.; Bonn, M. Molecular Modeling of Water Interfaces: From Molecular Spectroscopy to Thermodynamics. *J. Phys. Chem. B* **2016**, *120*, 3785−3796.
(36) Baer, M. D.; Kuo, I.-F. W.; Tobias, D. J.; Mundy, C. J. Toward a Unified Picture of the Water Self-Ions at the Air−Water Interface: A Density Functional Theory Perspective. *J. Phys. Chem. B* **2014**, *118*, 8364−8372.
(37) Kühne, T. D.; Pascal, T. A.; Kaxiras, E.; Jung, Y. New Insights into the Structure of the Vapor/Water Interface from Large-Scale First-Principles Simulations. *J. Phys. Chem. Lett.* **2011**, *2*, 105−113.
(38) Sulpizi, M.; Salanne, M.; Sprik, M.; Gaigeot, M.-P. Vibrational Sum Frequency Generation Spectroscopy of the Water Liquid−Vapor Interface from Density Functional Theory-Based Molecular Dynamics Simulations. *J. Phys. Chem. Lett.* **2013**, *4*, 83−87.
(39) Hsieh, C.-S.; Campen, R. K.; Vila Verde, A. C.; Bolhuis, P.; Nienhuys, H.-K.; Bonn, M. Ultrafast Reorientation of Dangling OH Groups at the Air-Water Interface Using Femtosecond Vibrational Spectroscopy. *Phys. Rev. Lett.* **2011**, *107*, 116102.
(40) Tong, Y.; Vila Verde, A.; Campen, R. K. The Free OD at the Air/D 2 O Interface Is Structurally and Dynamically Heterogeneous. *J. Phys. Chem. B* **2013**, *117*, 11753−11764.
(41) Hsieh, C.-S.; Campen, R. K.; Okuno, M.; Backus, E. H. G.; Nagata, Y.; Bonn, M. Mechanism of Vibrational Energy Dissipation of Free OH Groups at the Air−Water Interface. *Proc. Natl. Acad. Sci. U. S. A.* **2013**, *110*, 18780−18785.
(42) Nagata, Y.; Yoshimune, S.; Hsieh, C.; Hunger, J.; Bonn, M. Ultrafast Vibrational Dynamics of Water Disentangled by Reverse Nonequilibrium Ab Initio Molecular Dynamics Simulations. *Phys. Rev. X* **2015**, *5*, 021002.
(43) Stiopkin, I. V.; Weeraman, C.; Pieniazek, P. A.; Shalhout, F. Y.; Skinner, J. L.; Benderskii, A. V. Hydrogen Bonding at the Water Surface Revealed by Isotopic Dilution Spectroscopy. *Nature* **2011**, *474*, 192−195.
(44) Scatena, L. F.; Brown, M. G.; Richmond, G. L. Water at Hydrophobic Surfaces : Weak Hydrogen Bonding and Strong Orientation Effects. *Science* **2001**, *292*, 908−912.
(45) Du, Q.; Superfine, R.; Freysz, E.; Shen, Y. R. Vibrational Spectroscopy of Water at the Vapor/Water Interface. *Phys. Rev. Lett.* **1993**, *70*, 2313−2316.
(46) Ishiyama, T.; Imamura, T.; Morita, A. Theoretical Studies of Structures and Vibrational Sum Frequency Generation Spectra at Aqueous Interfaces. *Chem. Rev.* **2014**, *114*, 8447−8470.
(47) Wei, X.; Miranda, P. B.; Shen, Y. R. Surface Vibrational Spectroscopic Study of Surface Melting of Ice. *Phys. Rev. Lett.* **2001**, *86*, 1554−1557.
(48) Wei, X.; Shen, Y. R. Motional Effect in Surface Sum-Frequency Vibrational Spectroscopy. *Phys. Rev. Lett.* **2001**, *86*, 4799−4802.
(49) Rao, Y.; Tao, Y. S.; Wang, H. F. Quantitative Analysis of Orientational Order in the Molecular Monolayer by Surface Second Harmonic Generation. *J. Chem. Phys.* **2003**, *119*, 5226−5236.


DOI: 10.1021/acs.jctc.9b00253
*J. Chem. Theory Comput.* 2019, 15, 3836−3843

(50) Perakis, F.; De Marco, L.; Shalit, A.; Tang, F.; Kann, Z. R.; Kühne, T. D.; Torre, R.; Bonn, M.; Nagata, Y. Vibrational Spectroscopy and Dynamics of Water. *Chem. Rev.* **2016**, *116*, 7590−7607.
(51) Nihonyanagi, S.; Yamaguchi, S.; Tahara, T. Ultrafast Dynamics at Water Interfaces Studied by Vibrational Sum Frequency Generation Spectroscopy. *Chem. Rev.* **2017**, *117*, 10665−10693.
(52) Klimeš, J.; Michaelides, A. Perspective: Advances and Challenges in Treating van Der Waals Dispersion Forces in Density Functional Theory. *J. Chem. Phys.* **2012**, *137*, 120901.
(53) Johnson, E. R.; Becke, A. D. A Post-Hartree-Fock Model of Intermolecular Interactions: Inclusion of Higher-Order Corrections. *J. Chem. Phys.* **2006**, *124*, 174104.
(54) Chai, J.-D.; Head-Gordon, M. Long-Range Corrected Hybrid Density Functionals with Damped Atom−Atom Dispersion Corrections. *Phys. Chem. Chem. Phys.* **2008**, *10*, 6615.
(55) Berland, K.; Cooper, V. R.; Lee, K.; Schröder, E.; Thonhauser, T.; Hyldgaard, P.; Lundqvist, B. I. Van Der Waals Forces in Density Functional Theory: A Review of the VdW-DF Method. *Rep. Prog. Phys.* **2015**, *78*, 066501.
(56) Vydrov, O. A.; Voorhis, T. Van. Nonlocal Van Der Waals Density Functionals Based on Local Response Models. In *Fundamentals of Time-Dependent Density Functional Theory*; Marques, M. A. L., Maitra, N. T., Nogueira, F. M. S., Gross, E. K. U., Rubio, A., Eds.; Springer Berlin Heidelberg: Berlin, Heidelberg, 2012; pp 443−456.
(57) Hyldgaard, P.; Berland, K.; Schröder, E. Interpretation of van Der Waals Density Functionals. *Phys. Rev. B: Condens. Matter Mater. Phys.* **2014**, *90*, 075148.
(58) Vandevondele, J.; Krack, M.; Mohamed, F.; Parrinello, M.; Chassaing, T.; Hutter, J. Quickstep: Fast and Accurate Density Functional Calculations Using a Mixed Gaussian and Plane Waves Approach. *Comput. Phys. Commun.* **2005**, *167*, 103−128.
(59) Hutter, J.; Iannuzzi, M.; Schiffmann, F.; Vandevondele, J. Cp2k: Atomistic Simulations of Condensed Matter Systems. *Wiley Interdiscip. Rev. Comput. Mol. Sci.* **2014**, *4*, 15−25.
(60) Perdew, J. P.; Burke, K.; Ernzerhof, M. Generalized Gradient Approximation Made Simple. *Phys. Rev. Lett.* **1996**, *77*, 3865−3868.
(61) Zhang, Y.; Yang, W. Comment on "Generalized Gradient Approximation Made Simple. *Phys. Rev. Lett.* **1998**, *80*, 890.
(62) Vosko, S. H.; Wilk, L.; Nusair, M. Accurate Spin-Dependent Electron Liquid Correlation Energies for Local Spin Density Calculations: A Critical Analysis. *Can. J. Phys.* **1980**, *58*, 1200−1211.
(63) Goedecker, S.; Teter, M.; Hutter, J. Separable Dual-Space Gaussian Pseudopotentials. *Phys. Rev. B: Condens. Matter Mater. Phys.* **1996**, *54*, 1703−1710.
(64) Krack, M. Pseudopotentials for H to Kr Optimized for Gradient-Corrected Exchange-Correlation Functionals. *Theor. Chem. Acc.* **2005**, *114*, 145−152.
(65) Bussi, G.; Donadio, D.; Parrinello, M. Canonical Sampling through Velocity Rescaling. *J. Chem. Phys.* **2007**, *126*, 014101.
(66) Hasegawa, T.; Tanimura, Y. A Polarizable Water Model for Intramolecular and Intermolecular Vibrational Spectroscopies. *J. Phys. Chem. B* **2011**, *115*, 5545−5553.
(67) Ohto, T.; Usui, K.; Hasegawa, T.; Bonn, M.; Nagata, Y. Toward Ab Initio Molecular Dynamics Modeling for Sum-Frequency Generation Spectra; an Efficient Algorithm Based on Surface-Specific Velocity-Velocity Correlation Function. *J. Chem. Phys.* **2015**, *143*, 124702.
(68) Nagata, Y.; Hsieh, C.-S.; Hasegawa, T.; Voll, J.; Backus, E. H. G.; Bonn, M. Water Bending Mode at the Water−Vapor Interface Probed by Sum-Frequency Generation Spectroscopy: A Combined Molecular Dynamics Simulation and Experimental Study. *J. Phys. Chem. Lett.* **2013**, *4*, 1872−1877.
(69) Khatib, R.; Sulpizi, M. Sum Frequency Generation Spectra from Velocity-Velocity Correlation Functions. *J. Phys. Chem. Lett.* **2017**, *8*, 1310−1314.
(70) Nagata, Y.; Hasegawa, T.; Backus, E. H. G. G.; Usui, K.; Yoshimune, S.; Ohto, T.; Bonn, M. The Surface Roughness, but Not the Water Molecular Orientation Varies with Temperature at the Water-Air Interface. *Phys. Chem. Chem. Phys.* **2015**, *17*, 23559−23564.
(71) Schaefer, J.; Backus, E. H. G.; Nagata, Y.; Bonn, M. Both Inter- and Intramolecular Coupling of O−H Groups Determine the Vibrational Response of the Water/Air Interface. *J. Phys. Chem. Lett.* **2016**, *7*, 4591−4595.
(72) Smit, W. J.; Tang, F.; Sánchez, M. A.; Backus, E. H. G.; Xu, L.; Hasegawa, T.; Bonn, M.; Bakker, H. J.; Nagata, Y. Excess Hydrogen Bond at the Ice-Vapor Interface around 200 K. *Phys. Rev. Lett.* **2017**, *119*, 133003.
(73) Smit, W. J.; Tang, F.; Nagata, Y.; Sánchez, M. A.; Hasegawa, T.; Backus, E. H. G.; Bonn, M.; Bakker, H. J. Observation and Identification of a New OH Stretch Vibrational Band at the Surface of Ice. *J. Phys. Chem. Lett.* **2017**, *8*, 3656−3660.
(74) Du, Q.; Freysz, E.; Shen, Y. R. Surface Vibrational Spectroscopic Studies of Hydrogen Bonding and Hydrophobicity. *Science* **1994**, *264*, 826−828.
(75) Gan, W.; Wu, D.; Zhang, Z.; Feng, R.; Wang, H. Polarization and Experimental Configuration Analyses of Sum Frequency Generation Vibrational Spectra, Structure, and Orientational Motion of the Air/Water Interface. *J. Chem. Phys.* **2006**, *124*, 114705.
(76) Feng, R.-R.; Guo, Y.; Wang, H.-F. Reorientation of the "Free OH" Group in the Top-Most Layer of Air/Water Interface of Sodium Fluoride Aqueous Solution Probed with Sum-Frequency Generation Vibrational Spectroscopy. *J. Chem. Phys.* **2014**, *141*, 18C507.
(77) Wei, X.; Miranda, P. B.; Zhang, C.; Shen, Y. R. Sum-Frequency Spectroscopic Studies of Ice Interfaces. *Phys. Rev. B: Condens. Matter Mater. Phys.* **2002**, *66*, 085401.
(78) Asbury, J. B.; Steinel, T.; Kwak, K.; Corcelli, S. A.; Lawrence, C. P.; Skinner, J. L.; Fayer, M. D. Dynamics of Water Probed with Vibrational Echo Correlation Spectroscopy. *J. Chem. Phys.* **2004**, *121*, 12431−12446.
(79) McGuire, J. A.; Shen, Y. R. Ultrafast Vibrational Dynamics at Water Interfaces. *Science* **2006**, *313*, 1945−1948.
(80) Gulans, A.; Puska, M. J.; Nieminen, R. M. Linear-Scaling Self-Consistent Implementation of the van Der Waals Density Functional. *Phys. Rev. B: Condens. Matter Mater. Phys.* **2009**, *79*, 201105.
(81) Kelkkanen, A. K.; Lundqvist, B. I.; Nørskov, J. K. Density Functional for van Der Waals Forces Accounts for Hydrogen Bond in Benchmark Set of Water Hexamers. *J. Chem. Phys.* **2009**, *131*, 046102.
(82) Forster-Tonigold, K.; Groß, A. Dispersion Corrected RPBE Studies of Liquid Water. *J. Chem. Phys.* **2014**, *141*, 064501.
(83) Skinner, L. B.; Huang, C.; Schlesinger, D.; Pettersson, L. G. M.; Nilsson, A.; Benmore, C. J. Benchmark Oxygen-Oxygen Pair-Distribution Function of Ambient Water from x-Ray Diffraction Measurements with a Wide Q -Range. *J. Chem. Phys.* **2013**, *138*, 074506.


DOI: 10.1021/acs.jctc.9b00253
*J. Chem. Theory Comput.* 2019, 15, 3836−3843